PHYSICAL REVIEW E **76**, 061917 (2007)

Axial optical trapping efficiency through a dielectric interface

Antonio Alvaro Ranha Neves,[1,*] Adriana Fontes,[2] Carlos Lenz Cesar,[3] Andrea Camposeo,[1] Roberto Cingolani,[1] and Dario Pisignano[1]

[1]*National Nanotechnology Laboratory of CNR-INFM, Università del Salento, c/o Distretto Tecnologico ISUFI, via Arnesano, I-73100 Lecce, Italy*

[2]*Federal University of Pernambuco, Recife, Pernambuco, Brazil*

[3]*CePOF, Instituto de Física, Universidade Estadual de Campinas, Campinas, São Paulo, Brazil*

(Received 16 June 2007; revised manuscript received 12 September 2007; published 28 December 2007)

Axial trapping through a dielectric interface is investigated in the framework of the angular spectrum representation and of the generalized Lorenz-Mie theory. We determine the optical force for an arbitrarily polarized non-paraxial, strongly aberrated, axially symmetric focusing beam and apply this description to the case of an arbitrarily positioned dielectric microsphere, commonly employed in optical tweezers, not taking into account the contribution of evanescent waves at the interface. We derive the analytical expression of the force profile, finding that the incident polarization does not affect the axial optical force. In addition, we derive an approximated expression for the axial force as a function of beam displacement just outside the microsphere and we show how the information provided by the ripple structure of the optical trapping efficiency versus sphere displacement curve, due to the aberration effect, could be exploited to calibrate the bead axial position versus the experimental beam positioning controls.

DOI: 10.1103/PhysRevE.76.061917 PACS number(s): 87.80.Cc, 42.25.−p, 87.64.−t, 07.10.Pz

I. INTRODUCTION

Many developments have been reported in optical trapping in recent years [1–3]. One very important contribution of the optical tweezers technique is its ability to carry out mechanical measurements in the world of micro-organisms and cells, which could be correlated with biochemical information. For these measurements, the displacement of a bead, with typical size, a, in the range of a few micrometers, is the preferential force transducer, the accurate determination of the position and displacement of such a trapped sphere being crucial to extract physicochemical information [4–7]. In particular, recently Merenda *et al.* measured that neglecting the microsphere displacements, which occur along the optical axis (z direction) in correspondence to a change of the transversal position, would lead one to overestimate the maximal transverse trapping force up to 50% [8]. Gong *et al.*, using the drag force method, concluded that the maximum transverse trapping force is much larger than the measured escape force, usually considered to be the maximal transverse force [9].

To date, especially for single-molecule experiments, most of the studies are performed along the beam axis alone, due to ease of either beam manipulation, or specimen preparation, or data interpretation. Since the axial trapping efficiency is weaker than the radial counterpart, this generally requires a high numerical aperture (NA) and an oil immersion objective [8,10–16]. Typically, an oil immersion-objective (glass–oil–cover slip, with refractive index, $n_1 \approx 1.55$) on water ($n_2 \approx 1.33$) is employed, as schematized in Fig. 1. To measure the distance between the trapped sphere and the cover slip, an approach relying on detecting the small oscillations produced by interference between the forward-scattered light and the light reflected between the trapped bead and the planar cover glass surface, has been recently presented [17]. A different method, relying on unzipping a single DNA molecule, could also be used as a reference signal for calibrations in the axial direction [7].

Of course, in the presence of spherical aberrations due to the n_1-n_2 refractive index mismatch at the dielectric interface, the focal point, originated from the annular ring around the optical axis, is closer to the cover slip surface upon increasing the objective angle, α_1. Such an optical aberration, resulting in an elongated focal volume, is especially significant for three-dimensional imaging and optical data storage, and for laser trapping [18–24]. This effect, investigated applying vectorial and scalar theories [25–27], is also particularly important for measurements of low values of optical forces, where the specimen is trapped away from the boarders of the Neubauer chamber (~ 100 μm deep) in order to avoid boundary layer effects due to adhesion or viscous effects, consequently decreasing the trapping force.

A previous treatment of spherical aberrations on optical trapping, presented by Lock [28], used a focal beam description that does not completely satisfy Maxwell equations. Rohrbach and Stelzer [29] gave a detailed analysis of the trap stiffness in the presence of spherical aberrations based on the propagation of electromagnetic waves, valid for the Rayleigh ($a \ll \lambda$) regime, whereas other authors investigated the geometrical optics ($a \gg \lambda$) domain [30–32]. Ganic *et al.* solved the radiation trapping force numerically adopting the vecto-

*antonio.neves@unile.it

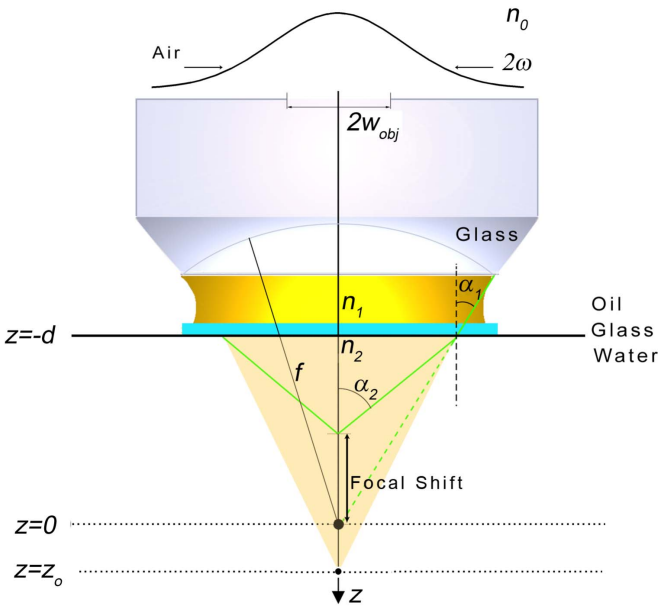

FIG. 1. (Color online) Geometrical scheme of light propagation through a refractive index mismatch interface. n_0, n_1, n_2: refractive indexes of air, glass, and water, respectively. f: focal length. ω: beam waist. w_{obj}: radius of the objective back aperture. z_o: nominal focal beam position. The immersion medium, between the objective and the cover slip, has the same refractive index, n_1, as glass. The black dot at $z=0$ will indicate in the following the microsphere center.

rial diffraction approach to represent the focused beam and arbitrary particle size [33].

Important, in the aberrated focal region, sharp fluctuations of the absolute electric field occur and, depending on the interface geometries, they can generate cusps, caustics, or other folds [34,35]. Several techniques have been employed to minimize the undesired effects of spherical aberration, both for imaging [36–38] and for optical trapping [23,31,39–41]. However, the electric field ripples, clearly appreciable also in the axial force curve, can be viewed as a natural ruler allowing one to exactly determine the axial distances and, consequently, to calibrate the beam positioning mechanisms (optics positions, microscope stage controls, etc.). Here we propose to exploit aberration to calibrate the axial trap distance, and a model is presented to take into account the ripple structure of the axial optical curve. We derive an expression for the aberrated axial force that, by comparison with analytical results, is shown to be able to effectively describe the system, especially upon decreasing the bead size, namely for Rayleigh experimental conditions, where the aberration effects are more critical. This expression can be used to fit experimental data, thus allowing one to determine the unknown axial calibration displacement parameters.

Concerning theories providing a description of the optical trapping of particles with arbitrary size, valid for Rayleigh and geometrical optics domain, the generalized Mie theory (GLMT) is the most adequate [42–44]. However, a main problem of GLMT stands in the nonparaxial beam description, which is fundamental to establish a true trapping in all three dimensions with only one beam. Indeed, paraxial approximations are no longer valid for typical experimental conditions, employing beams with NA>1, and microspheres with diameters up to the order of 10 wavelengths. These conditions require instead a full vectorial description of the incident beam, decomposed in partial waves, and preferably described in a coordinate system with the origin at the center of the bead, and not at the focus of the beam [45]. This has been achieved by the use of the $T-$matrix [46,47] and by GLMT [42–44], with the beam expressed by the angular spectrum representation [45,48]. In this work, an exact vectorial diffraction treatment of the aberrated axial optical force is presented, neglecting the contribution from evanescent waves, i.e., for distances larger than a few wavelengths from the interface, and valid for arbitrary sized dielectric spheres and focusing beam.

As conceptually expected, the resulting analytical expression for the axial trapping force is not affected by the incident polarization along the z axis.

II. THEORETICAL MODELING

Optical trapping is generally carried out within a nonabsorbing fluid of refractive index smaller than the employed dielectric particle, employing a high NA immersion microscope objective, with a glass cover slip and an immersion index matching fluid. The optically trapped object therefore suffers an aberration due to the refractive index mismatch at the interface (in our case, glass and water), which causes an apparent depth in the optical system [49]. The distance of this new focal point from the nonoptically perturbed medium is denominated focal shift. This effect is taken into account easily with the angular spectrum representation, since the plane interface is a surface of constant coordinate [49–55].

As schematized in Fig. 1, the origin of our coordinate system ($z=0$) is in the focal length, f, of the objective, and the interface between the two dielectric media, having refractive index n_1 and n_2, respectively, is located at $z=-d$ (z-axis positive in the direction of beam propagation). Both media are assumed to be linear, homogeneous, isotropic, and nonconducting. Assuming that the trapping focal beam position is a few wavelengths or larger from the interface (i.e., not taking into account contributions due to evanescent waves at the interface), we can apply the angular spectrum representation (also known as vectorial Debye diffraction theory or Debye integral) [56], weighting each ray by the Fresnel coefficients and applying the boundary conditions for the electric ($\mathbf{E}$) and magnetic ($\mathbf{H}$) fields at the interface. In this way we obtain the analytical expression of the transmitted electromagnetic fields $\mathbf{F}_2$, in terms of a field $\mathbf{F}=F_x\hat{\mathbf{x}}+F_y\hat{\mathbf{y}}$ incident on the objective. The components of the incident field, $\mathbf{F}$, in an aplanatic system, are indicated as $F_{x,y}=E_{x,y}$ for the electric field or $F_{x,y}=\pm H_{y,x}$ for the magnetic field, respectively. In cylindrical coordinates (ρ,φ,z), this reads as

$$\mathbf{F}_2(\rho,\varphi,z) = \frac{ik_2 f e^{-ik_2 f}}{2\pi}\int_0^{\alpha_{\max}} d\alpha_1 \sqrt{\cos\alpha_1}\,\sin\alpha_1 \exp[-id(k_1\cos\alpha_1 - k_2\cos\alpha_2)]$$
$$\times\exp[ik_2 z\cos\alpha_2]\int_0^{2\pi} d\beta \exp[ik_1\rho\sin\alpha_1\cos(\beta-\varphi)]$$
$$\times\left\{\begin{bmatrix}(t^{p,s}\cos\alpha_2 - t^{s,p})\cos^2\beta + t^{s,p} & (t^{p,s}\cos\alpha_2 - t^{s,p})\cos\beta\sin\beta \\ (t^{p,s}\cos\alpha_2 - t^{s,p})\cos\beta\sin\beta & (t^{p,s}\cos\alpha_2 - t^{s,p})\sin^2\beta + t^{s,p} \\ -t^{p,s}\sin\alpha_2\cos\beta & -t^{p,s}\sin\alpha_2\sin\beta\end{bmatrix}\begin{pmatrix}F_x\\F_y\end{pmatrix}\right\}, \quad (1)$$

where $\cos\alpha_2=[1-(n_1\sin\alpha_1/n_2)^2]^{1/2}$, β is the azimuthal objective angle, k_1 (k_2) indicates the modulus of the wave vector in the first (second) medium, t^s and t^p are the Fresnel transmission coefficients for s and p polarizations, and the left- and right-hand superscripts correspond to the electrical and to the magnetic fields, respectively. The Fresnel transmission coefficients are given by

$$t^s = \frac{2n_1\cos\alpha_1}{n_1\cos\alpha_1 + n_2\cos\alpha_2}, \quad t^p = \frac{2n_1\cos\alpha_1}{n_2\cos\alpha_1 + n_1\cos\alpha_2}. \quad (2)$$

Similar expressions were obtained by Egner and Török using the Fresnel-Kirchhoff or Debye integral approach [57,58]. The phase term in Eq. (1) represents the aberration function characterizing the spherical wave front distortion. From the radial components of the fields, one can then obtain the beam shape coefficients (BSC), $G_{nm}^{\mathrm{TM,TE}}$, corresponding to transversal electric (TE) and transversal magnetic (TM) multipoles, respectively ($n=1,\ldots,+\infty,-n\le m\le n$). The BSC for an axis-symmetric beam, following the procedure outlined in previous work [45], can be expressed in spherical coordinates (r,Ω), whose origin of coordinates is located at the center of the microsphere as follows:

$$G_{nm}^{\mathrm{TM,TE}} = \mp\frac{k_2 r}{j_n(k_2 r)F_o\sqrt{n(n+1)}}\int Y_{nm}^{*}\mathbf{F}\cdot\hat{\mathbf{r}}\,d\Omega$$
$$= \pm 4\pi i^{n-m}\left(\frac{(2n+1)(n-m)!}{4\pi n(n+1)(n+m)!}\right)^{1/2}\sqrt{\frac{n_0}{n_1}}ik_2 f e^{-ik_1 f}\exp(-im\phi_o)\int_0^{\alpha_{\max}} d\alpha_1\sqrt{\cos\alpha_1}\exp(-ik_2 z_o\cos\alpha_2)$$
$$\times\exp[-i(k_1\cos\alpha_1 - k_2\cos\alpha_2)d]\Bigg\{m^2 t^{s,p}\frac{J_m(k_2\rho_o\sin\alpha_2)}{k_2\rho_o\sin\alpha_2}P_n^m(\cos\alpha_2)$$
$$-t^{p,s}\sin^2\alpha_2 J_m'(k_2\rho_o\sin\alpha_2)P_n'^m(\cos\alpha_2), im\Bigg[t^{s,p}J_m'(k_2\rho_o\sin\alpha_2)P_n^m(\cos\alpha_2)$$
$$-t^{p,s}\sin^2\alpha_2\frac{J_m(k_2\rho_o\sin\alpha_2)}{k_2\rho_o\sin\alpha_2}P_n'^m(\cos\alpha_2)\Bigg]\Bigg\}\begin{pmatrix}\cos\phi_o & \sin\phi_o\\ \sin\phi_o & -\cos\phi_o\end{pmatrix}\begin{pmatrix}F_x\\F_y\end{pmatrix}. \quad (3)$$

Here, J_m are the Bessel functions of the first kind of mth order, Y_{nm} are spherical harmonics, P_n^m are the associate Legendre functions, $*$ denotes the complex conjugate, and (ρ_o,ϕ_o,z_o) are the nominal coordinates of the beam focal position with respect to the origin. The angular integration limit, $\alpha_{\max}$, is given by the condition of total internal reflection, $\alpha_{\max}=\sin^{-1}(n_2/n_1)$, lowering the effective NA of the objective. Equation (3), whose right-hand side involves a $(1\times2)(2\times2)(2\times1)$ matrix operation, generalizes the results of Ref. [45], since it also takes into account the effects of the refractive index mismatch.

Considering that the beam movement is restricted to be performed along the axial direction only, we can simplify the expression above, setting $\rho_o=0$. In this case, only the BSC with $m=\pm1$ remain [59,60], due to the limiting conditions imposed on the Bessel functions. Let us also suppose a transversal electromagnetic ($\mathrm{TEM}_{0,0}$) Gaussian beam amplitude, i.e., $F_i=F_o\exp[-(f\sin\alpha/\omega)^2]p_i$, where ω indicates the incident beam waist before entering the objective back aperture and p_i are the polarization components, which can be directly compared with experimental results. The two BSC are now reduced to a single one:

$$G_{n,\pm1}^{\mathrm{TM}} = (\pm p_x - ip_y)G_n^{\mathrm{TM}}, \quad G_{n,\pm1}^{\mathrm{TE}} = (\mp p_x + ip_y)G_n^{\mathrm{TE}}, \quad (4)$$

where

$$G_n^{\mathrm{TM,TE}} = \frac{i^n\sqrt{\pi}\sqrt{2n+1}}{n(n+1)}\sqrt{\frac{n_0}{n_1}}ik_2 f e^{-ik_1 f}\int_0^{\alpha_{\max}} d\alpha\sqrt{\cos\alpha}$$
$$\times\exp[-i(k_1\cos\alpha - k_2\cos\alpha_2)d]$$
$$\times\exp[-ik_2 z_o\cos\alpha_2]\exp[-(f\sin\alpha/\omega)^2]$$
$$\times[t^{s,p}P_n^1(\cos\alpha_2) - t^{p,s}\sin^2\alpha_2 P_n'^1(\cos\alpha_2)]. \quad (5)$$

TABLE I. Frequently used normalized Jones vectors.

Linear x polarization	Linear y polarization	Right circular polarization	Left circular polarization
$\begin{pmatrix}1\\0\end{pmatrix}$	$\begin{pmatrix}0\\1\end{pmatrix}$	$\frac{1}{\sqrt{2}}\begin{pmatrix}1\\i\end{pmatrix}$	$\frac{1}{\sqrt{2}}\begin{pmatrix}1\\-i\end{pmatrix}$

The symmetries for the BSC in Eq. (4) can now be explored for the special cases of linearly polarized and circularly polarized beams, replacing the (p_x,p_y) polarization vector by the appropriate Jones vector (Table I). For circular polarization we have only BSC with $m=+1$ or $m=-1$, which in a quantum interpretation corresponds to a discrete photon angular momentum of $\pm\hbar$ [61]. To determine the time averaged EM resultant force, **R**, on a dielectric sphere, we proceed by integrating the Minkowski form of the Maxwell stress tensor, T_{ij}, over the surface of a sphere in the far field [62],

$$R_i = \oint T_{ij} dA_j = \frac{1}{2}\mathrm{Re}\oint \left[\varepsilon E_i E_j^* + \mu H_i H_j^* - \frac{1}{2}(\varepsilon \mathbf{E}\cdot\mathbf{E}^* + \mu \mathbf{H}\cdot\mathbf{H}^*)\delta_{ij} \right] dA_j, \tag{6}$$

where ε and μ are the dielectric constant and the magnetic permeability, respectively. The Lorenz-Mie theory, according to which the fields are continuous inside and outside the sphere surface, leads to the following expression for the axial component of the optical force:

$$R_z = \frac{\varepsilon_2 |E_0|^2}{k_2^2}\mathrm{Re}\left(i\sum_{n=1} \frac{n(n+2)}{(n+1)\sqrt{(2n+1)(2n+3)}} \times [(a_{n+1} + a_n^* - 2a_{n+1}a_n^*)G_{n+1}^{\mathrm{TM}} G_n^{\mathrm{TM}^*} + (b_{n+1} + b_n^* - 2b_{n+1}b_n^*)G_{n+1}^{\mathrm{TE}} G_n^{\mathrm{TE}^*}] + \frac{i}{n(n+1)}(a_n + b_n^* - 2a_n b_n^*)G_n^{\mathrm{TM}} G_n^{\mathrm{TE}^*} \right)(|p_x|^2 + |p_y|^2). \tag{7}$$

Here a_n and b_n are the traditional Mie scattering coefficients for a dielectric sphere.

The previous equation is greatly simplified for the on-axis beam, since only the $m=\pm 1$ multipole coefficients are present, due to the BSC in Eq. (4). The R_z value is also independent of polarization, since the Jones vector is unitary by definition, i.e., no gain or loss in the axial trapping force occurs upon using a linear or circular polarized incident beam. Upon inserting Eq. (4) in Eq. (7), and using the definition of trapping efficiency [63], $Q_z = cR_z/Pn_2$, where c is the speed of light in vacuum and P indicates the laser power through the objective back aperture (radius$=w_{\mathrm{obj}}$) (Fig. 1), since the Gaussian beam tails are truncated by the finite aperture, one has finally,

$$Q_z = \frac{2}{(k_o\omega)^2 \pi n_2 [1 - \exp(-2w_{\mathrm{obj}}^2/\omega^2)]} \times \mathrm{Re}\left\{ i\sum_{n=1} \frac{n(n+2)}{(n+1)\sqrt{(2n+1)(2n+3)}} \times [(a_{n+1} + a_n^* - 2a_{n+1}a_n^*)G_{n+1}^{\mathrm{TM}} G_n^{\mathrm{TM}^*} + (b_{n+1} + b_n^* - 2b_{n+1}b_n^*)G_{n+1}^{\mathrm{TE}} G_n^{\mathrm{TE}^*}] + \frac{i}{n(n+1)}(a_n + b_n^* - 2a_n b_n^*)G_n^{\mathrm{TM}} G_n^{\mathrm{TE}^*} \right\}, \tag{8}$$

where k_o is the wave vector in air. This gives an adimensional quantity indicating the amount of momentum transferred from the beam onto the microsphere. This expression for the axial trapping efficiency does not take into account losses due to system absorption or to the actual microscope objective transmission, which experimentally are around 60% [1].

Furthermore, aiming to derive an approximate expression for the axial trapping efficiency of an aberrated system on a microsphere as a function of the axial distance, we start from Eq. (5), which is an integral equation for the beam axial position. In particular, we determine the points of stationary phase under the aperture angle integral [64], as recently applied to the analytical description of arbitrary strongly aberrated axially symmetric focusing by a sphere lens [35]. The axial optical force, Eq. (8), derives its oscillatory nature from the BSC of Eq. (5), which is of the kind $G_n^{\mathrm{TM,TE}} = \int_{x_1}^{x_2} f_n^{\mathrm{TM,TE}}(x)\exp[i\gamma g(x)]dx$ [65], where $\gamma \to \infty$. The method of stationary phase can be applied to evaluate the asymptotic behavior of the previous integral for the critical points of the first and second kind. In fact, calculation up to the critical points of the second kind is needed to obtain the ripple structure, since the optical force involves the product of this type of integral with its complex conjugate. This leads to

$$G_n^{\mathrm{TM,TE}} \approx \sqrt{\frac{2\pi}{\gamma |g''(x_c)|}} f_n^{\mathrm{TM,TE}}(x_c)\exp[i\gamma g(x_c) \pm i\pi/4] + \frac{1}{i\gamma}\left(\frac{f_n^{\mathrm{TM,TE}}(x_2)}{g'(x_2)}\exp[i\gamma g(x_2)] - \frac{f_n^{\mathrm{TM,TE}}(x_1)}{g'(x_1)}\exp[i\gamma g(x_1)] \right), \tag{9}$$

where the sign is taken depending on the sign of $g''(x_c)$, and x_c is the critical point in the integration interval. In a wave-theoretical context, the previous expression may be interpreted as phase interference from the diffractive wave [64]. The approximate and exact expressions for the BSC given by Eq. (9) and Eq. (5), respectively, are used in Eq. (8) to determine the optical force.

III. QUANTITATIVE RESULTS

Using numerical calculations based on the model described in the preceding section, we clarify how the aberrated axial trapping efficiency depends on the axial distance, and

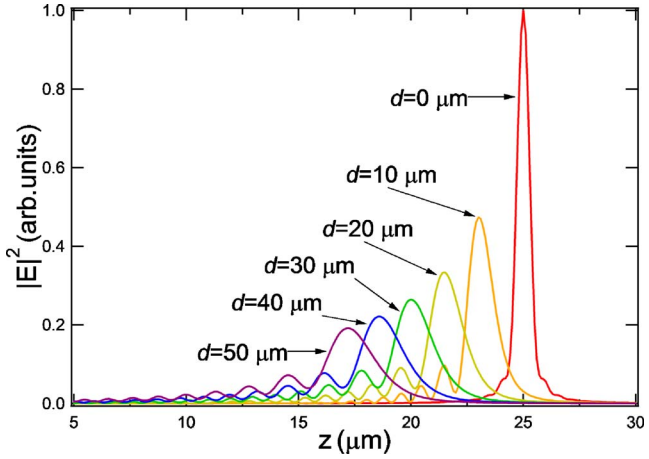

FIG. 2. (Color online) Numerically computed intensity of the electric field as a function of the coordinate, z, for a nominal beam coordinate $z_o=25$ μm, at different distances, d, between the unaberrated focal beam position and the dielectric interface.

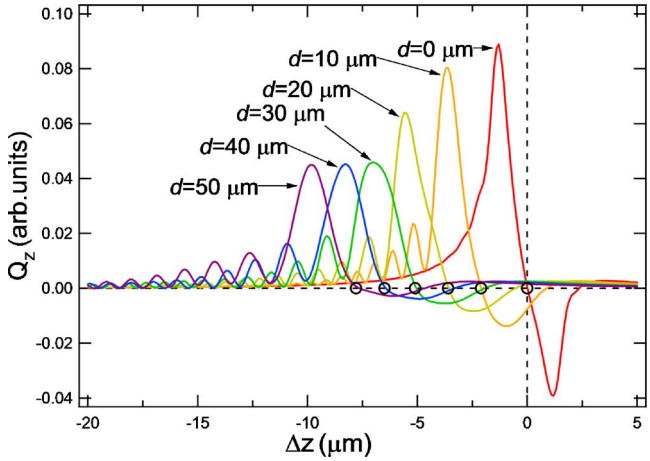

FIG. 3. (Color online) Axial trapping efficiency, Q_z, as a function of the displacement between the microsphere and nominal focal beam position ($\Delta_z=-z_0$), for a 2 μm polystyrene sphere, for different d values. Circles along the $Q_z=0$ line represent the stable trapping positions.

on the separation, d, between the n_1/n_2 dielectric interface and the origin of the coordinate system ($z=0$). The beam is moved axially with respect to the microsphere, which is placed at the origin, by changing the values of z_o. For instance, $z_o=0$ represents a beam nominally focused positioned at the center of the microsphere, while $d=0$ represents the case of a nonaberrated focal system. Simulations of the axial trapping efficiency achieved by an objective in an aplanatic system were performed for a variety of combinations of bead size and cover glass position. In particular, all of the simulations considered the trapping of a micrometer-sized spherical bead with an index of refraction, $n_b=1.59$ (polystyrene) in water ($n_2=1.33$), objective focal length, $f=1.7$ mm, back aperture radius, $w_{\mathrm{obj}}=2.5$ mm, with a trapping laser having $\lambda=800$ nm, and $\omega=2.5$ mm. The index of refraction of glass and of immersion oil, n_1, was taken as 1.51. These are typical values employed in experimental conditions.

The intensity behavior of the absolute electric field squared (nominally placed at $z_o=25$ μm) upon varying the axial distance, as determined by Eq. (1), is displayed in Fig. 2. The intensity profile is no longer symmetric along the optical axis, differently from the case of the unaberrated system ($d=0$). The observed oscillations are interpreted as due to constructive and destructive interference, because of the different propagation lengths of each plane wave after the mismatch interface [38,66].

These oscillations can be mapped onto the axial trapping efficiency through Eq. (8) as a function of the microsphere displacement with respect to the beam position. Since we placed the microsphere at the origin, such displacement is given by $\Delta z=-z_o$. For $d>0$, the trapping efficiency is reduced, as clearly observable from the absolute values of the minima, decreasing upon increasing the value of d (Fig. 3). Such reduction of the trapping efficiency with the increase of the trap depth originates from spherical aberrations, which focus the outermost rays of the beam in front of (namely, at a lower z value than) those in the center of the beam, thus creating an elongated focus. This eventually causes the peripheral rays to miss the bead as the cover glass is moved away from the interface, hence decreasing the resulting trapping efficiency.

Concomitantly, the escape force in the positive z direction decreases as the beam is displaced further into the medium [18,29,67]. The stable trapping positions, given by the axial coordinates where the axial trapping efficiency is zero and the $(\Delta z, Q_z)$ curve exhibits a negative slope, are evidenced in Fig. 3 with circles.

We also examined how the force curves are influenced by the size of microspheres. It can be observed (Fig. 4) that the periodicity of the $(\Delta z, Q_z)$ curve remains unchanged for different values of microsphere sizes, as described by Eq. (8). In addition, smaller microspheres ($a=0.5$ μm in Fig. 4) can exhibit more than one trapping position. The oscillations due to aberrations correspond to those observed in the electric field (Fig. 2). We also notice that the same argument about

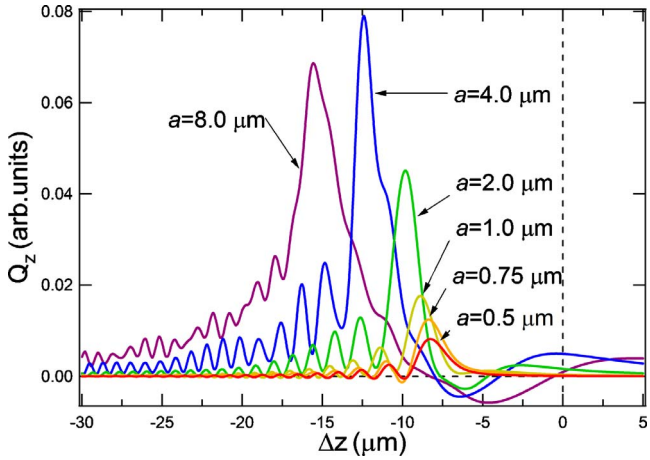

FIG. 4. (Color online) Axial optical trapping efficiency, Q_z, as a function of the beam focal position ($\Delta z=-z_0$), for polystyrene microspheres, for different bead sizes ($d=50$ μm).

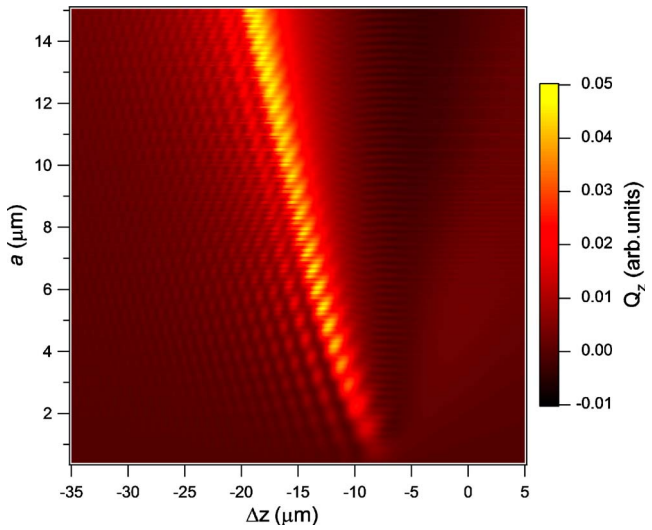

FIG. 5. (Color online) Two-dimensional plot of the axial optical trapping efficiency, Q_z, as a function of $\Delta z=-z_0$ (horizontal axis) and microsphere diameter (vertical axis). The well-defined ripple structure is clearly appreciable for smaller spheres (Rayleigh condition). The maximum axial trapping efficiency is indicated by the black region (negative force values) at the right of the high intensity peaks.

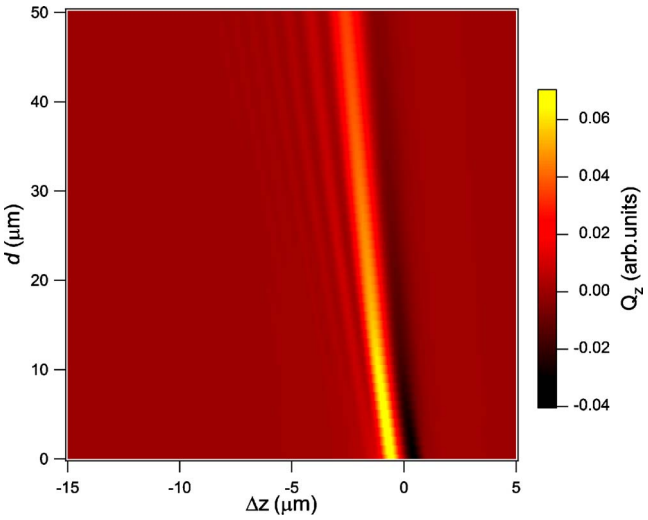

FIG. 6. (Color online) Two-dimensional plot of the axial optical trapping efficiency, Q_z, as a function of $\Delta z=-z_0$ (horizontal axis) and microsphere (with size $a=\lambda$) distance from cover slip (vertical axis). The ripple structure can be seen clearly as trapping depth increases.

the decrease of the trapping efficiency as in Fig. 3 also applies to the case in which the sphere diameter varies (see the Q_z minima in the $Q_z<0$ region in Fig. 4, whose absolute values increase upon increasing the bead size), i.e., better trapping occurs for larger microspheres in an aberrated system. Figure 5 shows the resulting ripple structure due to the aberration, which is more evident for smaller particles, as expected [23], and which exhibits more than one trapping region. Figure 6 shows instead that the ripple structure in the axial optical trapping efficiency profile, as a function of trapping depth (distance from the interface) for a microsphere, having $a=\lambda=800$ nm. Compared to the study by Ganic and co-workers [33], our work solves the trapping problem analytically up to the stage for which this is possible, thus greatly reducing the demand of computation time. In general, it is possible to solve part of the vectorial Debye theory, or even to determine the beam expansion coefficients finally obtaining only one numerical integral, analytically including the effects of aberration. In addition, these optical force calculations provide a full optical force curve versus beam focal position with respect to the microsphere, instead of particular points of the force curve.

Finally, in Fig. 7, we compare the oscillatory periodicity derived from the exact and approximated expressions of the axial trapping efficiency, namely plotting Eq. (8) and deriving Q_z from Eq. (9), respectively. Indeed, multiplying Eq. (9) by its complex conjugate allowed us to obtain a series of leading oscillatory terms that represents the ripple structure observed in the axial trapping efficiency curve,

$$Q_z(z_o) \propto A_0 \exp[-i\sqrt{(k_1^2-k_2^2)(2d-z_o)z_o}/n_1] + A_1 \exp[i(k_2-k_1)d - ik_2 z_o], \quad (10)$$

where A_i are the amplitudes that vary along the beam displacement direction. This expression can be used to describe measured oscillation of the axial force. From Fig. 7, we notice that the accordance between the exact and the approximate resulting curves improves upon decreasing the bead size, namely for Rayleigh experimental conditions, where the aberration effects are more critical, whereas the agreement between the resulting oscillatory periodicities is very good also for larger bead size (a). In particular, we point out that, once the ripple structure of the axial force is experimentally

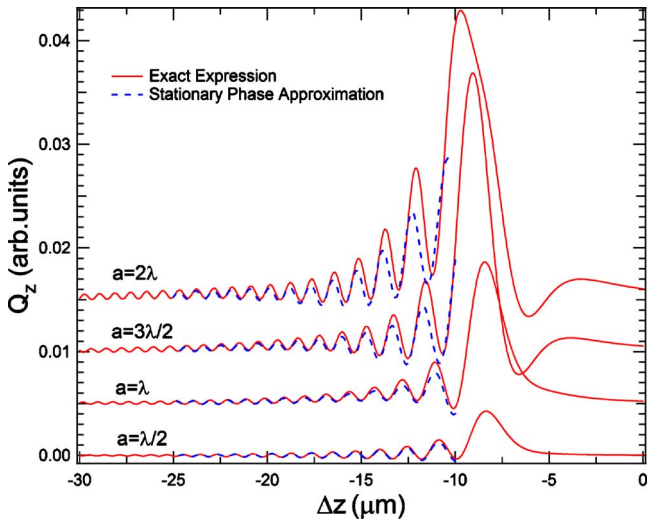

FIG. 7. (Color online) Axial optical trapping efficiency (red solid line) as a function of Δz for small microsphere diameters ($\lambda=800$ nm), interface distance, $d=50$ μm, and its stationary phase approximation, Eq. (9), in the ripple range (blue dashed line). Curves translated vertically by subsequent offsets of 0.05 for better clarity.

measured, one can use Eq. (10) to fit the data and also determine the calibration parameters needed to relate the nominal beam position (z_o) with the experimental motion controls. In fact, since z_o is related to the experiment controls on optics positions and microscope stage through a linear or a nonlinear function depending on the particular employed motion stage, one can determine the unknown parameters of this function by inserting it in Eq. (10), and then fitting the axial trapping efficiency oscillation ripples. Hence, the oscillation ripples constitute a natural role for axial displacement control calibration.

IV. CONCLUSIONS

The model here presented substantially extends previous reports [48], taking into account the effects of a refractive index mismatch in a typical trapping experiment, with a vectorial description of light. In this way, we have obtained two important results. First, the axial trapping efficiency can be determined for an arbitrary microsphere size and beam polarization. In particular, the resulting analytical expression demonstrates that the polarization does not affect the axial trapping efficiency, even when aberrations are taken into account.

Second, we describe the influence of spherical aberration, due to refractive index mismatch of medium and cover slip, on the optical force and on the trapping efficiency. We derive also an approximated expression for the axial force and we discuss how the information provided by the $(\Delta z, Q_z)$ ripple structure could be used to calibrate the axial position of a microsphere inside the immersion medium versus the experimental beam positioning. This calibration approach, working for an arbitrary depth, does not need to detect the interference between the sphere and cover slip [17], or to unzip a known DNA molecule [7]. It could be very useful, especially for dual optical trapping configuration, often preferable to single trapping setups, due to its ease of manipulating particles, beam coupling to resonance modes of microspheres, spectroscopic capability, noise reduction, and moreover allowing one to obtain a whole curve of the optical force as a function of the nominal beam position [48,68,69].

ACKNOWLEDGMENTS

This work was supported by the FIRB project "Laboratorio nazionale sulle nanotecnologie per la genomica e postgenomica" (NG-Laboratory).

[1] K. C. Neuman and S. M. Block, Rev. Sci. Instrum. **75**, 2787 (2004).
[2] D. G. Grier, Nature (London) **424**, 810 (2003).
[3] D. McGloin, Philos. Trans. R. Soc. London, Ser. A **364**, 3521 (2006).
[4] K. C. Vermeulen, G. J. L. Wuite, G. J. M. Stienen, and C. F. Schmidt, Appl. Opt. **45**, 1812 (2006).
[5] H. Kress, E. H. K. Stelzer, G. Griffiths, and A. Rohrbach, Phys. Rev. E **71**, 061927 (2005).
[6] J. K. Dreyer, K. Berg-Sørensen, and L. Oddershede, Appl. Opt. **43**, 1991 (2004).
[7] C. Deufel and M. D. Wang, Biophys. J. **90**, 657 (2005).
[8] F. Merenda, G. Boer, J. Rohner, G. Delacrétaz, and R. P. Salathé, Opt. Express **14**, 1685 (2006).
[9] Z. Gong, Z. Wang, Y. Li, L. Lou, and S. Xu, Opt. Commun. **273**, 37 (2007).
[10] M. D. Wang, M. J. Schnitzer, H. Yin, R. Landick, J. Gelles, and S. M. Block, Science **282**, 902 (1998).
[11] K. Adelman, A. La Porta, T. J. Santangelo, J. T. Lis, J. W. Roberts, and M. D. Wang, Proc. Natl. Acad. Sci. U.S.A. **99**, 13538 (2002).
[12] K. C. Neuman, E. A. Abbondanzieri, R. Landick, J. Gelles, and S. M. Block, Cell **115**, 437 (2003).
[13] A. Shundrovsky, T. J. Santangelo, J. W. Roberts, and M. D. Wang, Biophys. J. **87**, 3945 (2004).
[14] M. D. Wang, H. Yin, R. Landick, J. Gelles, and S. M. Block, Biophys. J. **72**, 1335 (1997).
[15] T. T. Perkins, R. V. Dalal, P. G. Mitsis, and S. M. Block, Science **301**, 1914 (2003).
[16] B. D. Brower-Toland, C. L. Smith, R. C. Yeh, J. T. Lis, C. L. Peterson, and M. D. Wang, Proc. Natl. Acad. Sci. U.S.A. **99**, 1960 (2002).
[17] K. C. Neuman, E. A. Abbondanzieri, and S. M. Block, Opt. Lett. **30**, 1318 (2005).
[18] M. J. Booth and T. Wilson, J. Biomed. Opt. **6**, 266 (2001).
[19] D. Day and M. Gu, Appl. Opt. **37**, 6299 (1998).
[20] I. Escobar, G. Saavedra, M. Martínez-Corral, and J. Lancis, J. Opt. Soc. Am. A **23**, 3150 (2006).
[21] A. Diaspro, S. Annunziata, and M. Robello, Microsc. Res. Tech. **51**, 464 (2000).
[22] A. C. Dogariu and R. Rajagopalan, Langmuir **16**, 2770 (2000).
[23] S. N. S. Reihani, M. A. Charsooghi, H. R. Khalesifard, and R. Golestanian, Opt. Lett. **31**, 766 (2006).
[24] E. Fällman and O. Axner, Appl. Opt. **42**, 3915 (2003).
[25] C. J. R. Sheppard and M. Gu, Appl. Opt. **30**, 3563 (1991).
[26] C. J. R. Sheppard and M. Gu, Opt. Commun. **88**, 180 (1992).
[27] C. J. R. Sheppard, M. Gu, K. Brain, and H. Zhou, Appl. Opt. **33**, 616 (1994).
[28] J. A. Lock, Appl. Opt. **43**, 2532 (2004).
[29] A. Rohrbach and E. H. K. Stelzer, Appl. Opt. **41**, 2494 (2002).
[30] X. C. Yao, Z. L. Li, H. L. Guo, B. Y. Cheng, and D. Z. Zhang, Chin. Phys. Lett. **18**, 432 (2001).
[31] X. C. Yao, Z. L. Li, H. L. Guo, B. Y. Cheng, X. H. Han, and D. Z. Zhang, Chin. Phys. **9**, 824 (2000).
[32] P. C. Ke and M. Gu, J. Mod. Opt. **45**, 2159 (1998).
[33] D. Ganic, X. Gan, and M. Gu, Opt. Express **12**, 2670 (2004).
[34] J. F. Nye, J. Opt. A, Pure Appl. Opt. **7**, 95 (2005).
[35] J. Kofler and N. Arnold, Phys. Rev. B **73**, 235401 (2006).
[36] M. J. Booth, M. A. A. Neil, and T. Wilson, J. Microsc. **192**, 90 (1998).
[37] C. J. de Grauw, J. M. Vroom, H. T. M. van der Voort, and H. C. Gerritsen, Appl. Opt. **38**, 5995 (1999).

[38] S. H. Wiersma, T. D. Visser, and P. Török, Opt. Lett. **23**, 415 (1998).
[39] T. Ota, T. Sugiura, S. Kawata, M. J. Booth, M. A. A. Neil, R. Juskaitis, and T. Wilson, Jpn. J. Appl. Phys. **42**, L701 (2003).
[40] E. Theofanidou, L. Wilson, W. J. Hossack, and J. Arlt, Opt. Commun. **236**, 145 (2004).
[41] S. N. S. Reihani and L. B. Oddershede, Opt. Lett. **32**, 1998 (2007).
[42] G. Gouesbet and G. Grehan, J. Opt. **13**, 97 (1982).
[43] G. Gouesbet, B. Maheu, and G. Grehan, J. Opt. Soc. Am. A **5**, 1427 (1988).
[44] B. Maheu, G. Gouesbet, and G. Grehan, J. Opt. **19**, 59 (1988).
[45] A. A. R. Neves, A. Fontes, L. A. Padilha, E. Rodriguez, C. H. B. Cruz, L. C. Barbosa, and C. L. Cesar, Opt. Lett. **31**, 2477 (2006).
[46] F. Borghese, P. Denti, and R. Saija, *Scattering from Model Nonspherical Particles* (Springer, Heidelberg, 2002).
[47] T. A. Nieminen, H. Rubinsztein-Dunlop, and N. R. Heckenberg, J. Quant. Spectrosc. Radiat. Transf. **79-80**, 1005 (2003).
[48] A. A. R. Neves, A. Fontes, L. de Y. Pozzo, A. A. de Thomaz, E. Chillce, E. Rodriguez, L. C. Barbosa, and C. L. Cesar, Opt. Express **14**, 13101 (2006).
[49] C. J. R. Sheppard and P. Török, J. Microsc. **185**, 366 (1997).
[50] T. D. Visser and S. H. Wiersma, J. Opt. Soc. Am. A **9**, 2034 (1992).
[51] L. Novotny and B. Hecht, *Principles of Nano-Optics* (Cambridge University Press, New York, 2006).
[52] S. Hell, G. Reiner, C. Cremer, and E. H. K. Stelzer, J. Microsc. **169**, 391 (1993).
[53] P. Török and P. Varga, Appl. Opt. **36**, 2305 (1997).
[54] S. H. Wiersma, P. Török, T. D. Visser, and P. Varga, J. Opt. Soc. Am. A **14**, 1482 (1997).
[55] P. Török, P. Varga, and G. Németh, J. Opt. Soc. Am. A **12**, 2660 (1995).
[56] M. Born and E. Wolf, *Principles of Optics*, 6th ed. (Pergamon, New York, 1980).
[57] A. Egner and S. W. Hell, J. Microsc. **193**, 244 (1999).
[58] P. Török, P. Varga, Z. Laczik, and G. R. Booker, J. Opt. Soc. Am. A **12**, 325 (1995).
[59] G. Gouesbet, J. A. Lock, and G. Grehan, Appl. Opt. **34**, 2133 (1995).
[60] G. Gouesbet, Appl. Opt. **35**, 1543 (1996).
[61] N. B. Simpson, K. Dholakia, L. Allen, and M. J. Padgett, Opt. Lett. **22**, 52 (1997).
[62] J. D. Jackson, *Classical Electrodynamics*, 3rd ed. (Wiley, New York, 1999).
[63] A. T. O'Neil and M. J. Padgett, Opt. Commun. **193**, 45 (2001).
[64] J. J. Stamnes, Opt. Express **10**, 740 (2002).
[65] Here, following a change of integration variable $x=\cos\alpha_1$, $f_n^{\mathrm{TM,TE}}(x)$ represents the amplitude that does not depend on either beam position z_o or displacement from cover slip d. The phase function, $g(x)$, is $(1-z_o/d)\sqrt{(n_2/n_1)^2-(1-x^2)}-x$, and $\gamma=k_1 d$. Note that some restrictions apply, so as to have a real critical point. We need $1>(1-z_o/d)>0$ and $1>(n_2/n_1)>0$; this consequently restricts the interval of the beam displacement variable (z_o) to the region of the observed oscillations.
[66] P. Török, P. Varga, A. Konkol, and G. R. Booker, J. Opt. Soc. Am. A **13**, 2232 (1996).
[67] S. Nemoto and H. Togo, Appl. Opt. **37**, 6386 (1996).
[68] A. Fontes, A. A. R. Neves, W. L. Moreira, A. A. de Thomaz, L. C. Barbosa, C. L. Cesar, and A. M. de Paula, Appl. Phys. Lett. **87**, 221109 (2005).
[69] J. R. Moffitt, Y. R. Chemla, D. Izhaky, and C. Bustamante, Proc. Natl. Acad. Sci. U.S.A. **103**, 9006 (2006).